ACSNANO

www.acsnano.org

ARTICLE

Block Copolymer Nanocomposites with High Refractive Index Contrast for One-Step Photonics

Dong-Po Song, Cheng Li, Wenhao Li, and James J. Watkins*

Department of Polymer Science and Engineering, University of Massachusetts Amherst, 120 Governors Drive, Amherst, Massachusetts 01003, United States

Supporting Information

ABSTRACT: Photonic crystals (PhCs) prepared using the self-assembly of block copolymers (BCPs) offer the potential for simple and rapid device fabrication but typically suffer from low refractive index contrast ($\Delta n \leq 0.1$) between the phase-segregated domains. Here, we report the simple fabrication of BCP-based photonic nanocomposites with large differences in refractive index ($\Delta n > 0.27$). Zirconium oxide (ZrO_2) nanoparticles coated with gallic acid are used to tune the optical constants of the target domains of self-assembled (polynorbornene-*graft*-poly(*tert*-butyl acrylate))-*block*-(polynorbornene-*graft*-poly(ethylene oxide)) (PtBA-*b*-PEO) brush block copolymers (BBCPs). Strong hydrogen-bonding interactions between the ligands on ZrO_2 and PEO brushes of the BBCPs enable selective incorporation and high loading of up to 70 wt % (42 vol %) of the ZrO_2 nanoparticles within the PEO domain, resulting in a significant increase of refractive index from 1.45 to up to 1.70. Consequently, greatly enhanced reflection at approximately 398 nm (increases of ~250%) was observed for the photonic nanocomposites (domain spacing = 137 nm) relative to that of the unmodified BBCPs, which is consistent with numeric modeling results using transfer matrix methods. This work provides a simple strategy for a wide range tuning of optical constants of BCP domains, thereby enabling the design and creation of high-performance photonic coatings for various applications. The large refractive index contrast enables high reflectivity while simultaneously reducing the coating thickness necessary, compared to pure BCP systems.

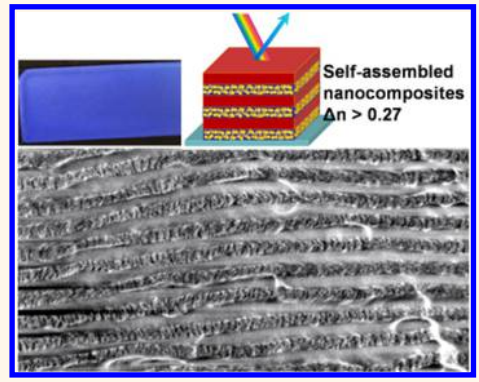

KEYWORDS: *photonic nanocomposites, block copolymer, self-assembly, high refractive index contrast*

Precise control over the alignment of functional nanomaterials such as semiconductor, plasmonic, and dielectric nanoparticles (NPs) is highly desirable for a variety of important applications ranging from sensors, to energy and memory storage devices, to photovoltaic, nonlinear optical, plasmonic, and other electronic nanodevices.[1−13] The directed self-assembly of NPs using block copolymer (BCP) as the template provides a simple strategy for the low-cost "bottom up" fabrication of the next-generation hybrid materials that combine the mechanical property and processability of polymers with the attractive physical properties of well-aligned NP arrays.[11−13]

Linear BCPs (LBCPs) have been widely used for NP patterning in the past two decades, as they can self-assemble into periodic spherical, cylindrical, bicontinuous, and lamellar morphologies.[14−35] The selective incorporation of NPs within a specific domain of a microphase-separated LBCP enables the organization of NP arrays at the nanoscale level, resulting in periodic hybrid materials with greatly enhanced mechanical, optical, and electric properties.[11−13] The dispersion of NPs in BCPs is dependent on a balance between the enthalpic contribution due to NP/BCP interactions and the entropic penalty arising from polymer chain stretching for incorporation of NPs. In systems with weak NP/polymer chain interactions,[14−23] the chain stretching penalty can dominate, resulting in barriers to the formation of well-ordered composites containing significant quantities of NPs. By contrast, surface modification of NPs using ligands that exhibit favorable interactions with BCP segments is an effective way to sequester NPs within the target domains while maintaining strong phase segregation. Favorable NP/BCP interactions can be realized *via* hydrogen bonding (H-bonding)[24−31] and *via* ionic interactions.[32] In addition, the alignment of NPs was also achieved using small molecules as the intermediates that exhibit H-bonding with BCP segments and neutral interaction with NPs.[33−35] Here the small-molecule additives serve to mitigate the entropic penalties of NP addition.

Received: October 16, 2015
Accepted: December 29, 2015
Published: December 29, 2015

© 2015 American Chemical Society

DOI: 10.1021/acsnano.5b06525
ACS Nano 2016, 10, 1216−1223

Photonic structures such as one-dimensional photonic crystals (1D PhC) have been proposed and successfully created *via* the self-assembly of BCPs, opening a simple route to flexible photonic devices or coatings in an inexpensive and scalable way but at present subject to several limitations.[36−39] The domain spacing (*d*-spacing) of a LBCP is typically a few tens of nanometers, which is not large enough to open a photonic band gap in the visible light region. Therefore, additives have been used to swell the target domains such as homopolymers,[40] solvents,[41] liquid crystals,[42] ionic liquid,[43] and silica.[44] Recently, 1D PhCs were reported through the rapid self-assembly of brush block copolymers (BBCPs) with high molecular weights up to 10^3 kg/mol and large domain spacing over 100 nm.[45−52] However, the refractive index contrast (Δn) between phase-segregated domains of BCPs is typically no more than 0.1 in both cases, which will limit their utility in future potential applications such as optical filters, reflectors, sensors, and optical cavities.

The selective incorporation of metal NPs into certain domains of self-assembled LBCPs has been used to modify the optical constants of target domains.[53,54] Nevertheless, the preparation of useful photonic nanocomposites based on BCPs has remained challenging due to two severe limitations. First, the domain size of an LBCP is typically less than 50 nm, which is not large enough to reflect visible light.[10−35] Second, the loading concentration of NPs and the tuning of optical constants of BCP domains have been limited.[53,54] Recently, we reported photonic nanocomposites containing high concentrations of gold NPs from the self-assembly of (polynorbornene-*graft*-poly(styrene))-*block*-(polynorbornene-*graft*-poly(ethylene oxide)) BBCPs ($(PNB\text{-}PS_{3.5k})_n$-*b*-$(PNB\text{-}PEO_{2k})_m$).[55] Although the metallodielectric structure showed interesting photonic behavior, the absorption of the visible light by the metal component leads to a limited reflection.

Here we address these limitations *via* the self-assembly of BBCP-based nanocomposites stabilized by strong enthalpic interactions between the BBCP matrix and zirconium oxide (ZrO_2) NPs, which are transparent to visible light (see Scheme 1). This approach yields well-ordered photonic nanocomposites (PhCs) with an exceptional high refractive index contrast ($\Delta n > 0.27$). The ZrO_2 NPs are coated with gallic acid (GA), which exhibits strong H-bonding interactions with the PEO side chains of the BBCPs. As a result, the loading concentration of NPs in the nanocomposites can be up to 40 wt % (17 vol %) based on the mass of the composites, corresponding to 70 wt % (42 vol %) in the target domain without aggregation of the NPs. The reflection from the highly filled nanocomposites is up to 250% stronger relative to that measured for the parent BBCPs. Transfer matrix methods were used to model the optical characteristics of the composites as a function of refractive index contrast and showed a good agreement with the experimental results.

RESULTS AND DISCUSSION

Metal oxide NPs have been used to enhance the refractive index contrast between the alternating low/high-index materials in polymer 1D PhCs prepared by sequential spin coating, as they often have high refractive indices ($n > 2$) and can be transparent in visible light.[56,57] Our group recently reported the successful fabrication of strain-tunable 1D PhCs based on slide-ring elastomer nanocomposites containing commercially available ZrO_2 NPs.[57] However, the fabrication process requires multiple steps of spin-coating and curing and is time-consuming when making large-area coatings. In this work, we aim to create 1D PhCs *via* self-assembly of BBCP-based nanocomposites using ZrO_2 NPs to tune optical constants of the target domains over broad ranges. Compared with LBCPs, there are many advantages of using BBCPs to fabricate photonic structures such as the large lattice spacing, rapid self-assembly kinetics,[46−52] the enhanced capability for accommodating high loading of inorganic NPs,[55,58] and the long-range ordering.[58] Over 14 years ago, the Thomas group reported the tuning of the refractive index *via* the selective incorporation of gold NPs within the BCP domain.[53,54] Nevertheless, the core concentration of the gold NPs was briefly limited in less than 5 wt %,[53] and the tuning of the refractive index was limited. In addition, metal NPs are not ideal for photonic crystal fabrication, as the strong absorption of visible light by the metal component will lead to a great loss of light. A long annealing process of up to several days was also required for the LBCP blends to achieve ordered structure,[53] which has been a barrier for low-cost and scalable manufacturing. For comparison, well-ordered structures can be achieved within a few minutes for the bottle brush systems, benefiting from the much fewer polymer chain entanglements relative to that of the linear analogues.[46−52,55,58]

Scheme 1. (a) Surface modification of ZrO_2 NPs *via* ligand exchange with gallic acid (GA); (b) BBCP-based photonic structures (1D PhC) with large differences in refractive index ($\Delta n > 0.27$) fabricated *via* the co-assembly of asymmetric PtBA-*b*-PEO BBCPs (29.0 vol % < f_{PEO} < 32.7 vol %) and the modified ZrO_2 NPs (NP/GA). The high loading concentration of the modified NPs selectively within the PEO domain greatly enhances the effective refractive index contrast between PtBA and PEO/NP domains, leading to significantly enhanced reflection from the lamellar structures.

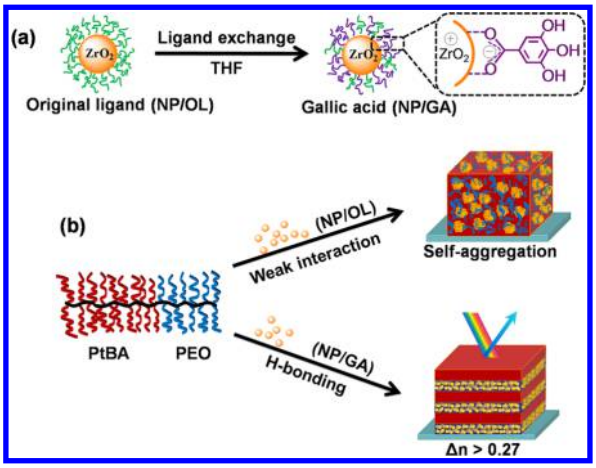

The BBCPs are well-defined (polynorbornene-*graft*-poly(*tert*-butyl acrylate))-*block*-(polynorbornene-*graft*-poly(ethylene oxide)) BCPs ($(PNB\text{-}PtBA_{8.2k})_n$-*b*-$(PNB\text{−}PEO_{5k})_m$) synthesized by sequential ring-opening metathesis polymerization (ROMP). The detailed synthetic procedures were reported in our recent publication.[58] The chemical structure of the BBCPs was characterized by FTIR and ^1H and ^{13}C NMR spectra, as shown in Figures S1−S3 (Supporting Information). Molecular weight information for the polymer series was obtained by gel permeation chromatography (GPC) and is summarized in Table 1. GPC IR traces (Figure S4) exhibit unimodal molecular weight distributions of the obtained

DOI: 10.1021/acsnano.5b06525
ACS Nano 2016, 10, 1216−1223

Table 1. Molecular Weight Information for the (Polynorbornene-*graft*-poly(tert-butyl acrylate))-*block*-(polynorbornene-*graft*-poly(ethylene oxide)) Copolymers

sample	M_n[a] (kg/mol)	PDI[a]	DP[b] PtBAMM	DP[b] PEOMM	f_{PEO}[c]	*d*-spacing[d] (nm)
BBCP-**A**	1590	1.15	128	108	32.3	91
BBCP-**B**	2150	1.08	172	148	32.7	133
BBCP-**C**	2760	1.05	233	169	29.0	196

[a]Molecular weight and polydispersity index as measured by GPC-MALLS. [b]Approximation of the size of each block as calculated using NMR and GPC results. [c]Volume fraction of PEO as calculated according to ^{1}H NMR. [d]The domain spacing (*d*-spacing) as determined by SAXS and USAXS data in Figure 1.

BBCPs, and the polydispersity indices (PDIs) are less than 1.2 (Table 1), indicating a good control over the copolymerization reactions. The volume fraction of the PEO block (f_{PEO}) was controlled from 29.0 to 32.7 vol %, as calculated according to the ^{1}H NMR spectra. These asymmetric PtBA-*b*-PEO BBCPs were designed for the accommodation of high loadings of NPs within the PEO domains while keeping a volume balance between PtBA and PEO/NP blocks in order to generate well-ordered lamellar morphologies in highly filled nanocomposites.

Small-angle X-ray scattering (SAXS) was used to characterize the bulk morphology and *d*-spacings of the PtBA-*b*-PEO BBCPs. Bulk samples were prepared in stainless steel washers that were sandwiched between Kapton films and heated at 100 °C under vacuum for 14 h before SAXS measurements were taken. As shown in Figure 1a, the SAXS profile of BBCP-**A**

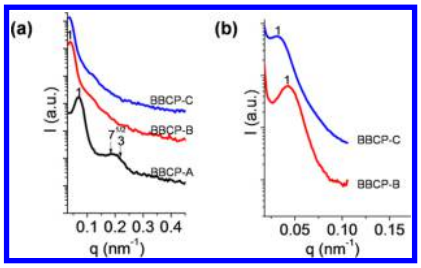

Figure 1. (a) SAXS profiles of BBCP-A, -B, and -C showing the increased *d*-spacing with the increased molecular weight of BBCP. (b) USAXS profiles of BBCP-B and -C showing the primary order peaks at small *q* values.

shows a sharp primary order peak at a scattering vector (q) of 0.069 nm^{-1}, indicating a strong phase separation of the BBCP into a periodic nanostructure with a *d*-spacing of 91 nm ($d = 2\pi/q$). A broad, higher scattering peak centered at $7^{1/2} < q < 3$ was also observed, indicative of randomly distributed spheres or cylinders.[59] A cylindrical morphology was confirmed by transmission electron microscopy (TEM) of the microtomed sample BBCP-**A** (Figure S5). For BBCP-**B** and -**C**, worm-like morphologies were observed in the TEM (Figure S5). The *d*-spacing of BBCP-**B** or -**C** was too large to be detected by conventional SAXS. Therefore, the *d*-spacing was obtained using ultra-small-angle X-ray scattering (USAXS in Figure 1b) and increased from 91 nm to 196 nm as the molecular weight increased from 1590 kg/mol to 2760 kg/mol (Table 1). BBCP-**B** and -**C**, with *d*-spacings greater than 100 nm, were chosen as the candidates for the fabrication of photonic nanocomposites.

Hydrogen-bonding interactions between NP additives and the BBCP host were employed to avoid NP self-aggregation and achieve large NP loadings while maintaining a well-ordered morphology. Surface modification was carried out on ZrO_2 NPs through ligand exchange with gallic acid. As shown in Scheme 1a, the surface of the modified ZrO_2 NPs is mostly covered by the carboxylic acid groups of GA with the phenol groups directed toward the periphery. This was confirmed by FTIR spectra (Figure 2) in which an evident peak shift of the C═O

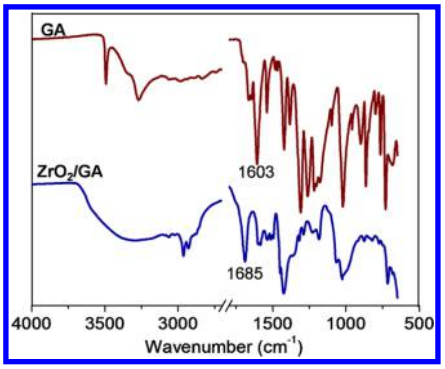

Figure 2. FTIR spectra of GA and modified ZrO_2 NPs (ZrO_2/GA) showing different peak positions of the C═O groups.

group was observed after the adsorption of the carbonyl group onto the NP surface.[60] The weight percentages of inorganic components before (86%) and after (82%) surface modification were determined by thermogravimetric analysis (TGA in Figure S6). Figure 3 shows the TEM micrograph of the modified ZrO_2 NPs with an average core diameter of approximately 6.1 nm, as indicated by the histogram (inset).

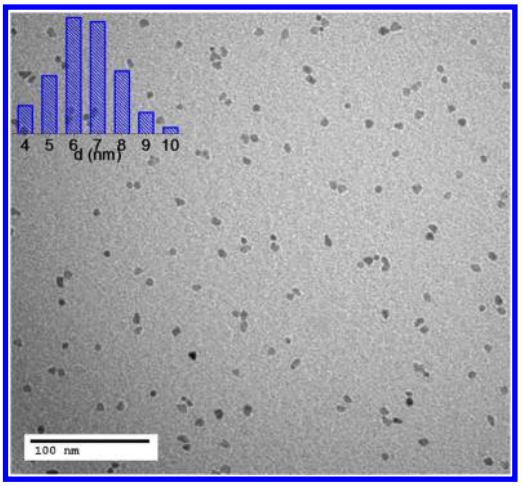

Figure 3. TEM micrograph of ZrO_2 NPs and the size distribution (inset). The average core diameter is 6.1 ± 1.5 nm, obtained by image analysis using ImageJ.

For the BBCP-NP composites, we typically prepared a 1.5% (w/v) polymer solution in anhydrous tetrahydrofuran (THF) admixed with ZrO_2 NPs in the desired proportions. Herein the weight percentage (wt %) of NPs in the composites is based on the mass of the NP core and ligand shell, while the volume percentage (vol %) of NPs (core + ligand) can be estimated using the TGA data and the densities of the components and is provided in parentheses following the NP wt % for each composite (see details in the Supporting Information). The morphologies of the BBCP-NP composites were determined by USAXS and TEM. As shown in Figure 4a, no peaks indicative of an ordered morphology were observed in the 1D USAXS

DOI: 10.1021/acsnano.5b06525
ACS Nano 2016, 10, 1216−1223

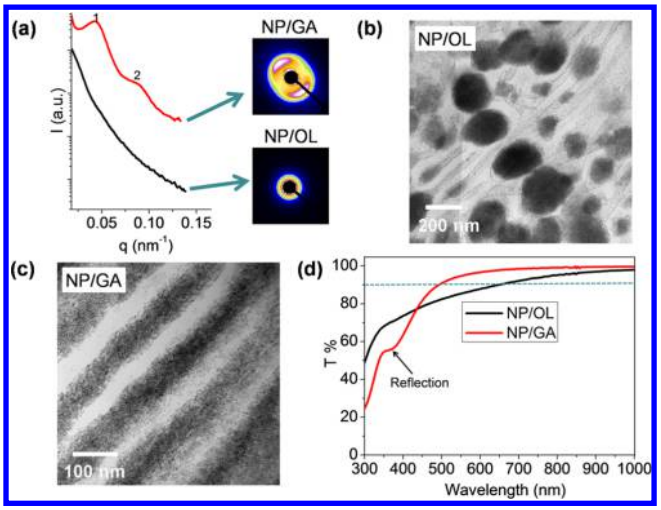

Figure 4. Significantly improved dispersion of ZrO_2 NPs in BBCP-C *via* strong H-bonding interactions. The composite films contain the same concentration (20 wt %) of ZrO_2 NPs before (NP/OL) and after (NP/GA) surface modification: (a) 1D USAXS profiles and the corresponding 2D scattering patterns; (b, c) TEM micrographs without staining; (d) transmission spectra using a glass substrate as the reference.

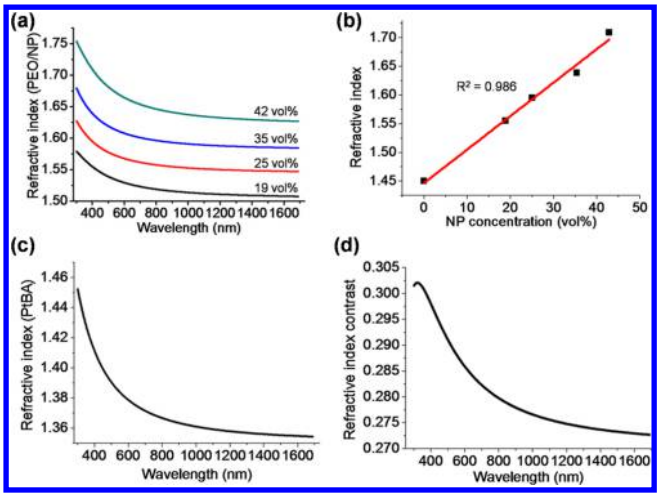

Figure 5. (a) Effective refractive index of blends of homopolymer PEO with different loading percentages of modified NPs including 42 wt % (19 vol %), 51 wt % (25 vol %), 63 wt % (35 vol %), and 70 wt % (42 vol %). (b) Effective refractive index as a function of NP concentration at 400 nm. (c) Refractive index of homopolymer PtBA as a function of wavelength. (d) Refractive index contrast (Δn) between PtBA and PEO/NP at an NP concentration of 70 wt %.

profile of the composite sample containing unmodified ZrO_2 NPs (NP/original ligand (OL)). In contrast, 1D SAXS of the composites containing the same loading concentration of the modified NPs (NP/GA) shows two well-defined peaks centered at $1q$ and $2q$, indicating a well-ordered lamellar morphology (see Scheme 1b). Moreover, a long-range directional order was observed in the lamellar morphology as indicated by the anisotropic 2D USAXS pattern (Figure 4a). The significant difference between the two samples was confirmed by TEM (Figure 4b *vs* c). The NPs are severely aggregated in the composite sample containing NP/OL, and large NP clusters of over 200 nm in diameter were observed (Figure 4b). The dispersion of NPs was dramatically improved by introducing strong H-bonding interactions between NPs and BBCPs. As shown Figure 4c, no NP aggregation was observed in the composite sample containing NP/GA, suggesting that the strong H-bonding interactions between GA on NPs and PEO side chains of the PtBA-*b*-PEO BBCPs can efficiently stabilize the highly filled composites. This is consistent with the previous studies of NP addition in LBCP systems.[27−31] Figure 4d shows that the composite film with a good dispersion of NPs is highly transparent in visible light (T% > 90%), while the sample containing aggregated NP clusters is subjected to scattering losses of light and shows a much lower transmittance.

The refractive index of the NP/PEO domain in BBCP composites at various loadings of ZrO_2 NPs was measured using variable-angle spectroscopic ellipsometry (VASE) for blends of homopolymer PEO containing the same amounts of NPs (Figure 5). Figure 5a shows the refractive indices of PEO/NP blends over a wavelength range from 300 to 1690 nm. It is evident that the refractive index of the PEO layer can be increased by incorporating ZrO_2 NPs, resulting in an enhanced refractive index contrast between the alternating PtBA and PEO/NP layers in the composites. As shown in Figure 5b, the refractive index of PEO/NP ($n_{PEO/NP}$) increased linearly (R^2 = 0.986) with the increasing NP volume fraction (f_{NP}) according to eq 1:

$$n_{PEO/NP} = 0.58 f_{NP} + 1.45. \quad (1)$$

This is consistent with our previous observation of a linear relationship between NP loading and the refractive index of the resulting blends.[57] A refractive index of up to 1.70 was observed at 400 nm for a PEO/NP blend containing 70 wt % (42 vol %) NPs. In addition, the refractive index of the PtBA domain was determined *via* VASE measurements on homopolymer PtBA. Figure 5c shows the refractive indices at different wavelengths from UV to IR. The refractive index contrast between PtBA and PEO/NP (70 wt %) layers is demonstrated in Figure 5d, and a value of up to 0.30 was obtained at 400 nm. The large difference (Δn > 0.27) between two alternating layers of 1D PhCs will greatly improve the performance of BCP-based photonic coatings.

Photonic composite films prepared by the self-assembly of PtBA-*b*-PEO BBCP-**B** and the modified ZrO_2 NPs were prepared through a simple solution cast on glass substrates followed by thermal annealing at 100 °C for about 14 h (Figure 6). A neat polymer film was also prepared as a control sample using the same fabrication procedure. The photographs of these photonic films (Figure 6a) show a significant difference between the neat polymer film and the composites. There is only a light blue color observed in the neat polymer film, while the composite films exhibited strong reflected light. The reflection measurements were performed on a UV/vis/NIR spectrometer equipped with an "integrating sphere" diffuse reflectance accessory at an incident angle of 8°. The reflectance obtained is a sum of reflected light from an area as large as 15 × 7 mm^2, which is the incident beam area. Reflection spectra (Figure 6b) confirmed the substantially increased reflectance (250% improvement) from 12% to 42% in the composite sample containing 30 wt % (12 vol %) of the ZrO_2 NPs, corresponding to 56 wt % (29 vol %) in the PEO domain. The refractive index of the PEO/NP domain was 1.62, as calculated using eq 1, while the refractive index of the PtBA domain was 1.41, as measured by VASE, resulting in a refractive index contrast up to 0.21 for the composites containing 30 wt % of

DOI: 10.1021/acsnano.5b06525
ACS Nano 2016, 10, 1216−1223

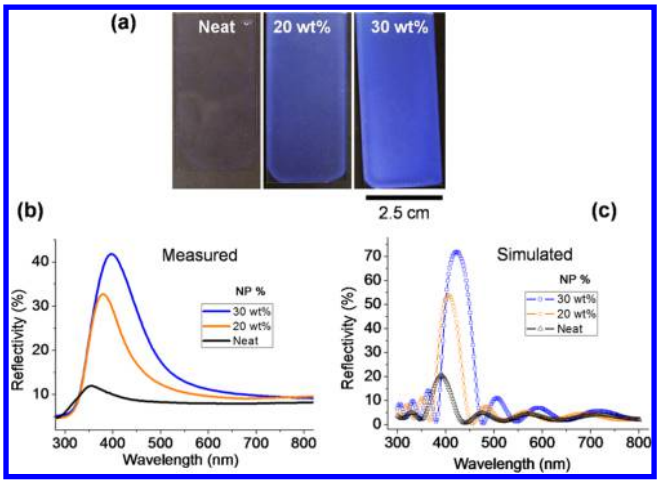

Figure 6. (a) Photographs of photonic films prepared *via* the self-assembly of BBCP-B and the modified NPs at different concentrations of 20 wt % (7.2 vol %) and 30 wt % (12 vol %). The photographs were taken on a black background under fluorescent light. (b, c) Measured and simulated reflection as a function of wavelength showing greatly enhanced reflectance *via* adding modified ZrO_2 NPs.

ZrO_2 NPs. Numerical modeling using transfer matrix methods was employed to describe the influence of refractive index contrast on reflectance assuming that all the samples have the same number of bilayers (see details in the Supporting Information). The simulated results (Figure 6c) indicate a greatly enhanced reflectivity (260%) upon adding 30 wt % of the ZrO_2 NPs to the BBCP, which show a good agreement with the experimental results (Figure 6b).

The *d*-spacing and morphology of the photonic films based on BBCP-**B** were characterized by SAXS and USAXS. As shown in Figure 7a, there is a broad peak centered at q = 1.04

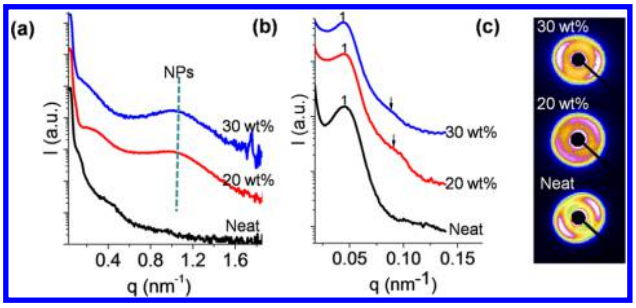

Figure 7. (a) SAXS, (b) USAXS profiles, and (c) 2D USAXS patterns of the photonic films obtained *via* the self-assembly of BBCP-B and modified NPs, corresponding to the samples in Figure 6.

in the 1D SAXS profiles of the composite samples, indicating an average NP size of approximately 6.0 nm, which is very close to the value obtained from TEM image analysis (Figure 3). The *d*-spacing of these samples was too large, and the primary ordering peak was overlapping with the beamstop of SAXS. Therefore, USAXS was used to verify the *d*-spacing. Figure 7b shows the evident primary order peaks, and a slight increase of the *d*-spacing from 133 to 137 nm was observed when increasing the NP concentration from 0 to 30 wt %. There are also higher order peaks at 2q, which can be seen in the 1D USAXS profiles of the composite samples, indicating a lamellar morphology. Moreover, a long-range directional order was observed as indicated by the anisotropic 2D USAXS patterns in Figure 7c. The well-ordered lamellar morphology was further confirmed by TEM and cross-sectional FESEM (Figure 8).

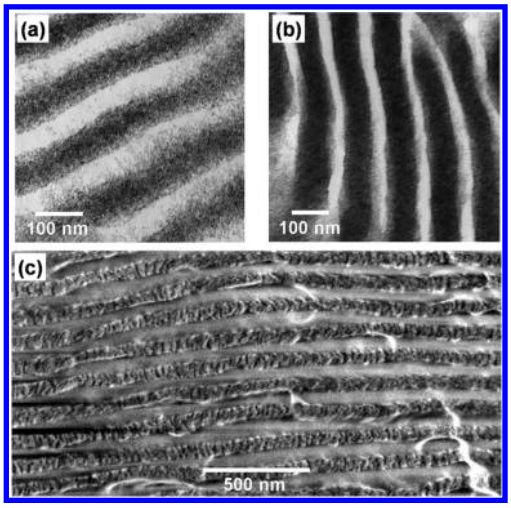

Figure 8. Structural characterization of the photonic films obtained from the self-assembly of BBCP-B and modified NPs (Figure 6). TEM micrographs of the photonic composite films containing different concentrations of NPs: (a) 20 wt % (7.2 vol %); (b) 30 wt % (12 vol %). (c) Cross-sectional FESEM micrograph of the composite sample containing 30 wt % NPs.

TEM characterization was carried out on the composite samples prepared by microtoming without staining. The contrast observed in the TEM images is due to the selective incorporation of ZrO_2 NPs within PEO domains, and the PEO/NP domains appear as the dark regions (Figure 8a and b). TEM showing a larger area of the composite sample containing 30 wt % NPs can be found in Figure S7, indicating a well-ordered lamellar morphology. Figure 8c shows the representative cross-sectional field emission scanning electron microscopy (FESEM) image of the composite film containing 30 wt % of ZrO_2 NPs. A well-ordered lamellar morphology was observed in a large area consistent with the USAXS results (Figure 7). The selective incorporation of NPs into BCP domains enabled the wide tuning of optical constants of target domains, providing a simple strategy for the design and fabrication of photonic composite materials or coatings.

Figure 9 shows the reflection spectra of the composite films prepared from self-assembly of BBCP-**C** and the modified ZrO_2 NPs. Similar to the composite films based on BBCP-**B**, a significant increase of reflectance was achieved in composites containing ZrO_2 NPs. A high loading concentration of up to 40 wt % (17 vol %) NPs in the composites was achieved without NP aggregation, corresponding to 70 wt % (42 vol %) within the PEO domain (see calculation details in the Supporting Information). The refractive index of the PEO/NP domain was 1.70, as calculated using eq 1, resulting in a large refractive index contrast up to 0.29 between PtBA and PEO/NP domains. In comparison with the composites containing 30 wt % NPs, no further increase of reflectance and a blue shift of the reflection peak from 390 nm to 348 nm were observed when increasing the NP concentration to 40 wt %, suggesting a possible morphology change in the composites. TEM micrographs of the composite samples containing various loading concentrations of NPs can be found in Figure S8 and confirmed the good dispersion of NPs in the highly filled nanocomposites

DOI: 10.1021/acsnano.5b06525
ACS Nano 2016, 10, 1216−1223

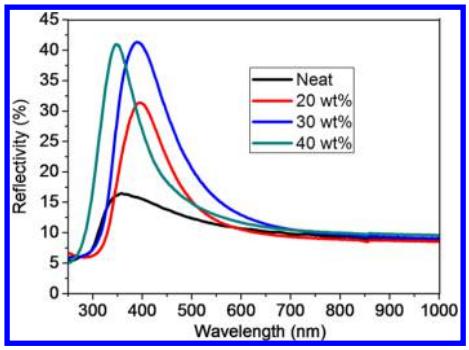

Figure 9. Reflection as a function of wavelength for blends of BBCP-C with different concentrations of modified NPs such as 20 wt % (7.2 vol %), 30 wt % (12 vol %), and 40 wt % (17 vol %), corresponding to 45 wt % (21 vol %), 58 wt % (32 vol %), and 70 wt % (42 vol %) within the PEO domain.

and an irregular distorted morphology observed in some areas of the sample containing 40 wt % of NPs. It may be possible to preserve strong order in the composite at NP loadings greater than 30 wt % by adjusting the volume fraction of PEO in the host BBCP.

CONCLUSION

A high refractive index contrast between different BCP domains is highly desirable for the low-cost "bottom up" fabrication of high-performance photonic materials. In this work, we demonstrated the fabrication of BCP-based photonic nanocomposites with large differences in refractive index (Δn > 0.27). Metal oxide NPs with high refractive indices were selectively incorporated within BCP domains under high loading concentrations without aggregation while maintaining a well-ordered morphology, resulting in BCP domains with widely tunable refractive indices from 1.45 to over 1.70. The composite films with a high refractive index contrast exhibited greatly enhanced reflection of up to 250% larger relative to that of the parent BBCP films, which has been well explained by transfer matrix simulations. This work provides a simple route to achieve homogeneous distribution and high loading of metal oxide nanocrystals within BCP domains *via* strong NP/BCP enthalpic interactions and to tune the optical constant of BCP domains for flexible photonic coatings or devices. In addition, the multilayered arrangement of the nanocrystals with high dielectric constants may be useful as next-generation materials for the fabrication of energy storage devices such as high-performance capacitors.

EXPERIMENTAL SECTION

Surface Modification of ZrO_2 NPs. Zirconium oxide nanocrystals dispersed in toluene were purchased from Pixelligent. The toluene solution was evaporated under nitrogen flow, and the dried NP solid was redispersed in THF, affording a clear solution. The concentration of the solution is 20 mg/mL. The surface modification was carried out simply by adding 5 wt % of gallic acid relative to the mass of all the components in the solution (see Scheme 1a). The resulting mixture was stirred for about 30 min, and the replacement of the original ligands by gallic acid was rapid and efficient (see details in the discussion part). The resulting solution was used for sample preparation without further purifications.

Preparation of NP/BCP Blends. Appropriate amounts of BBCPs were weighed and dissolved in anhydrous THF followed by adding NP solutions in the same solvent to form about 1.5% (wt/v) stock solutions. The THF solutions were cast through 0.45 μm PTFE filters onto horizontal glass substrates, which were covered immediately with glass Petri dishes. After solvent evaporation, the dried films were annealed at 100 °C under vacuum for 14 h. We note that the evaporation of THF solutions was carried out under a nitrogen atmosphere to control humidity below 20%. For SAXS sample preparation, the composite films were removed from glass substrates using a razor blade and filled in a washer at 110 °C. The resulting bulk samples were subsequently sealed using Kapton films and then cooled to room temperature in air before SAXS measurement. The sample thickness was approximately 0.60 mm. The anisotropic 2D SAXS patterns (Figure 4a and 7c) correspond to the bulk sample in washer, indicating a long-range order of the nanocomposites.

Preparation of NP/PEO Homopolymer Blends. PEO (2 kg/mol) from Sigma was blended with the modified ZrO_2 NPs in THF at different loading concentrations. The concentration of the resulting solution was around 10 mg/mL. Thin films on a silicon substrate for variable-angle spectroscopic ellipsometry measurements were prepared by spin coating at 3000 rpm, affording film thicknesses ranging from 73 to 83 nm. The thin films were subsequently put on a hot plate at 80 °C for about 5 min before VASE measurements.

Characterization. ^{1}H NMR spectroscopy was recorded in $CDCl_3$ using a Bruker Avance DPX 500 NMR spectrometer. Gel permeation chromatography of the brush BCPs was carried out in THF on two PLgel 10 μm mixed-B LS columns (Polymer Laboratories) connected in series with a DAWN EOS multiangle laser light scattering (MALLS) detector and an RI detector. No calibration standards were used for the bottle brush copolymers, and dn/dc values were obtained for each injection by assuming 100% mass elution from the columns. Thermogravimetric analysis experiments were performed on a TGA2950 thermogravimetric analyzer with a heating rate of 10 °C/min under air. Fourier transform infrared spectroscopy (FTIR) measurements were performed using a PerkinElmer FTIR spectrometer with an ATR crystal window. Small-angle X-ray scattering measurements were performed with a Ganesha SAXS-LAB using a 0.154 nm (Cu K radiation) X-ray, a sample-to-detector distance of 1491 mm, and an X-ray beam size of 0.04 mm^2. Ultra-small-angle X-ray scattering measurements were performed using a Xeuss USAXS equipment at the Changchun Institute of Applied Chemistry (CIAC) in China. The wavelength of the X-ray was 0.154 nm, the beam area was 0.6 × 0.6 mm^2, and the sample-to-detector distance was 6558 mm. Transmission electron microscopy measurements were conducted with a JEOL 2000FX TEM operated at an accelerating voltage of 200 kV. Composite samples were embedded in epoxy and cured at room temperature overnight. Thin sections of approximately 50 nm in thickness for microscopy were prepared using a Leica Ultracut UCT microtome equipped with a Leica EM FCS cryogenic sample chamber operated at −80 °C. FESEM measurements were carried out on a FEI Magellan 400 FESEM. The composite sample was cryofractured in liquid nitrogen to afford the cross sections for SEM. VASE measurements were performed on a J. A. Woollam RC2-DI ellipsometry with variable angles at 55°, 60°, 65°, and 70°. The refractive index was obtained by using a Cauchy model for data fitting in the wavelength range from 300 to 1690 nm. Reflection and transmission measurements on the samples were performed on a PerkinElmer LAMBDA 1050 UV/vis/NIR spectrometer, equipped with a 150 mm integrating sphere diffuse reflectance accessory. All reflection measurements were referenced to a Spectralon reflectance standard with a reflectance of over 99%. The light beam area was 7 mm in width and 15 mm in height.

ASSOCIATED CONTENT

Supporting Information

The Supporting Information is available free of charge on the ACS Publications website at DOI: 10.1021/acsnano.5b06525.

^{1}H and ^{13}C NMR spectra, FTIR spectrum, GPC traces, and TEM images of the brush block copolymers; TGA of zirconium oxide nanoparticles; TEM images of nanocomposites; and transfer matrix simulations (PDF)

DOI: 10.1021/acsnano.5b06525
ACS Nano 2016, 10, 1216−1223

AUTHOR INFORMATION

Corresponding Author

*E-mail: watkins@polysci.umass.edu. Tel: 413-545-2569. Fax: 413-545-0082.

Notes

The authors declare no competing financial interest.

ACKNOWLEDGMENTS

The authors acknowledge the use of the Xeuss USAXS equipment at the Changchun Institute of Applied Chemistry (CIAC) in China. We thank Nan Zheng and Prof. Yongfeng Men of CIAC for their assistance with the USAXS experiments. This work was supported by the NSF Center for Hierarchical Manufacturing at the University of Massachusetts (CMMI-1025020).

REFERENCES

(1) Choi, C. L.; Alivisatos, A. P. From Artificial Atoms to Nanocrystal Molecules: Preparation and Properties of More Complex Nanostructures. *Annu. Rev. Phys. Chem.* **2010**, *61*, 369−389.
(2) Talapin, D. V.; Lee, J.-S.; Kovalenko, M. V.; Shevchenko, E. V. Prospects of Colloidal Nanocrystals for Electronic and Optoelectronic Applications. *Chem. Rev.* **2010**, *110*, 389−458.
(3) Huynh, W. U.; Dittmer, J. J.; Alivisatos, A. P. Hybrid Nanorod-Polymer Solar Cells. *Science* **2002**, *295*, 2425−2427.
(4) Lopes, W. A.; Jaeger, H. M. Hierarchical Self-Assembly of Metal Nanostructures on Diblock Copolymer Scaffolds. *Nature* **2001**, *414*, 735−738.
(5) De Rosa, C.; Auriemma, F.; Di Girolamo, R.; Pepe, G. P.; Napolitano, T.; Scaldaferri, R. Enabling Strategies in Organic Electronics Using Ordered Block Copolymer Nanostructures. *Adv. Mater.* **2010**, *22*, 5414−5419.
(6) Xiang, J.; Lu, W.; Hu, Y.; Wu, Y.; Yan, H.; Lieber, C. M. Ge/Si Nanowire Heterostructures as High-Performance Field-Effect Transistors. *Nature* **2006**, *441*, 489−493.
(7) Briseno, A. L.; Yang, P. Optoelectronics: Combining Chemical Worlds. *Nat. Mater.* **2009**, *8*, 7−8.
(8) Lin, Y.; Lim, J. A.; Wei, Q.; Mannsfeld, S. C. B.; Briseno, A. L.; Watkins, J. J. Cooperative Assembly of Hydrogen-Bonded Diblock Copolythiophene/Fullerene Blends for Photovoltaic Devices with Well-Defined Morphologies and Enhanced Stability. *Chem. Mater.* **2012**, *24*, 622−632.
(9) Wei, Q. S.; Lin, Y.; Anderson, E. R.; Briseno, A. L.; Gido, S. P.; Watkins, J. J. Additive-Driven Assembly of Block Copolymer−Nanoparticle Hybrid Materials for Solution Processable Floating Gate Memory. *ACS Nano* **2012**, *6*, 1188−1194.
(10) Bockstaller, M. R.; Mickiewicz, R. A.; Thomas, E. L. Block Copolymer Nanocomposites: Perspectives for Tailored Functional Materials. *Adv. Mater.* **2005**, *17*, 1331−1349.
(11) Orilall, M. C.; Wiesner, U. Block Copolymer Based Composition and Morphology Control in Nanostructured Hybrid Materials for Energy Conversion and Storage: Solar Cells, Batteries, and Fuel Cells. *Chem. Soc. Rev.* **2011**, *40*, 520−535.
(12) Kao, J.; Thorkelsson, K.; Bai, P.; Rancatore, B. J.; Xu, T. Toward Functional Nanocomposites: Taking the Best of Nanoparticles, Polymers, and Small Molecules. *Chem. Soc. Rev.* **2013**, *42*, 2654−2678.
(13) Sarkar, B.; Alexandridis, P. Block Copolymer−Nanoparticle Composites: Structure, Functional Properties, and Processing. *Prog. Polym. Sci.* **2015**, *40*, 33−62.
(14) Lee, J. Y.; Thompson, R. B.; Jasnow, D.; Balazs, A. C. Entropically Driven Formation of Hierarchically Ordered Nanocomposites. *Phys. Rev. Lett.* **2002**, *89*, 155503.
(15) Bockstaller, M. R.; Lapetnikov, Y.; Margel, S.; Thomas, E. L. Size-Selective Organization of Enthalpic Compatibilized Nanocrystals in Ternary Block Copolymer/Particle Mixtures. *J. Am. Chem. Soc.* **2003**, *125*, 5276−5277.
(16) Chiu, J. J.; Kim, B. J.; Kramer, E. J.; Pine, D. J. Control of Nanoparticle Location in Block Copolymers. *J. Am. Chem. Soc.* **2005**, *127*, 5036−5037.
(17) Lin, Y.; Böker, A.; He, J. B.; Sill, K.; Xiang, H. Q.; Abetz, C.; Li, X. F.; Wang, J.; Emrick, T.; Long, S.; Wang, Q.; Balazs, A.; Russell, T. P. Self-Directed Self-Assembly of Nanoparticle/ Copolymer Mixtures. *Nature* **2005**, *434*, 55−59.
(18) Balazs, A. C.; Emrick, T.; Russell, T. P. Nanoparticle Polymer Composites: Where Two Small Worlds Meet. *Science* **2006**, *314*, 1107−1110.
(19) Kim, B. J.; Chiu, J. J.; Yi, G. R.; Pine, D. J.; Kramer, E. J. Nanoparticle-Induced Phase Transitions in Diblock-Copolymer Films. *Adv. Mater.* **2005**, *17*, 2618−2622.
(20) Kim, B. J.; Bang, J.; Hawker, C. J.; Kramer, E. J. Effect of Areal Chain Density on the Location of Polymer-Modified Gold Nanoparticles in A Block Copolymer Template. *Macromolecules* **2006**, *39*, 4108−4114.
(21) Kim, B. J.; Bang, J.; Hawker, C. J.; Chiu, J. J.; Pine, D. J.; Jang, S. G.; Yang, S. M.; Kramer, E. J. Creating Surfactant Nanoparticles for Block Copolymer Composites Through Surface Chemistry. *Langmuir* **2007**, *23*, 12693−12703.
(22) Chiu, J. J.; Kim, B. J.; Yi, G. R.; Bang, J.; Kramer, E. J.; Pine, D. J. Distribution of Nanoparticles in Lamellar Domains of Block Copolymers. *Macromolecules* **2007**, *40*, 3361−3365.
(23) Kim, B. J.; Fredrickson, G. H.; Kramer, E. J. Effect of Polymer Ligand Molecular Weight on Polymer-Coated Nanoparticle Location in Block Copolymers. *Macromolecules* **2008**, *41*, 436−447.
(24) Noro, A.; Matsushita, Y.; Lodge, T. P. Thermoreversible Supramacromolecular Ion Gels *via* Hydrogen Bonding. *Macromolecules* **2008**, *41*, 5839−5844.
(25) Noro, A.; Matsushita, Y.; Lodge, T. P. Gelation Mechanism of Thermoreversible Supramacromolecular Ion Gels *via* Hydrogen Bonding. *Macromolecules* **2009**, *42*, 5802−5810.
(26) Dobrosielska, K.; Takano, A.; Matsushita, Y. Creation of Hierarchical Nanophase-Separated Structures *via* Supramacromolecular Self-Assembly from Two Asymmetric Block Copolymers with Short Interacting Sequences Giving Hydrogen Bonding Interaction. *Macromolecules* **2010**, *43*, 1101−1107.
(27) Jang, S. G.; Kramer, E. J.; Hawker, C. J. Controlled Supramolecular Assembly of Micelle-Like Gold Nanoparticles in PS-b-P2VP Biblock Copolymers *via* Hydrogen Bonding. *J. Am. Chem. Soc.* **2011**, *133*, 16986−16996.
(28) Lin, Y.; Daga, V. K.; Anderson, E. R.; Gido, S. P.; Watkins, J. J. Nanoparticle-Driven Assembly of Block Copolymers: A Simple Route to Ordered Hybrid Materials. *J. Am. Chem. Soc.* **2011**, *133*, 6513−6516.
(29) Jang, S. G.; Khan, A.; Hawker, C. J.; Kramer, E. J. Morphology Evolution of PS-b-P2VP Diblock Copolymers *via* Supramolecular Assembly of Hydroxylated Gold Nanoparticles. *Macromolecules* **2012**, *45*, 1553−1561.
(30) Yao, L.; Lin, Y.; Watkins, J. J. Ultra High Loading of Nanoparticles into Ordered Block Copolymer Composites. *Macromolecules* **2014**, *47*, 1844−1849.
(31) Song, D. P.; Wang, X.; Lin, Y.; Watkins, J. J. Synthesis and Controlled Self-Assembly of UV-Responsive Gold Nanoparticles in Block Copolymer Templates. *J. Phys. Chem. B* **2014**, *118*, 12788−12795.
(32) Warren, S. C.; Messina, L. C.; Slaughter, L. S.; Kamperman, M.; Zhou, Q.; Gruner, S. M.; DiSalvo, F. J.; Wiesner, U. Ordered Mesoporous Materials from Metal Nanoparticle-Block Copolymer Self-Assembly. *Science* **2008**, *320*, 1748−1752.
(33) Zhao, Y.; Thorkelsson, K.; Mastroianni, A. J.; Schilling, T.; Luther, J. M.; Rancatore, B. J.; Matsunaga, K.; Jinnai, H.; Wu, Y.; Poulsen, D.; Fréchet, J. M. J.; Alivisatos, A. P.; Xu, T. Small-Molecule-Directed Nanoparticle Assembly towards Stimuli-Responsive Nanocomposites. *Nat. Mater.* **2009**, *8*, 979−985.
(34) Kao, J.; Bai, P.; Lucas, J. M.; Alivisatos, A. P.; Xu, T. Size-Dependent Assemblies of Nanoparticle Mixtures in Thin Films. *J. Am. Chem. Soc.* **2013**, *135*, 1680−1683.

DOI: 10.1021/acsnano.5b06525
ACS Nano 2016, 10, 1216−1223

(35) Kao, J.; Xu, T. Nanoparticle Assemblies in Supramolecular Nanocomposite Thin Films: Concentration Dependence. *J. Am. Chem. Soc.* **2015**, *137*, 6356−6365.
(36) Fink, Y.; Urbas, A. M.; Bawendi, M. G.; Joannopoulos, J. D.; Thomas, E. L. Block Copolymers as Photonic Bandgap Materials. *J. Lightwave Technol.* **1999**, *17*, 1963.
(37) Valkama, S.; Kosonen, H.; Ruokolainen, J.; Haatainen, T.; Torkkeli, M.; Serimaa, R.; Brinke, G. T.; Ikkala, O. Self-Assembled Polymeric Solid Films with Temperature-Induced Large and Reversible Photonic-Bandgap Switching. *Nat. Mater.* **2004**, *3*, 872−876.
(38) Lee, J. H.; Koh, C. Y.; Singer, J. P.; Jeon, S.; Maldovan, M.; Stein, O.; Thomas, E. L. Ordered Polymer Structures for the Engineering of Photons and Phonons. *Adv. Mater.* **2014**, *26*, 532−569.
(39) Stefik, M.; Guldin, S.; Vignolini, S.; Wiesner, U.; Steiner, U. Block Copolymer Self-Assembly for Nanophotonics. *Chem. Soc. Rev.* **2015**, *44*, 5076−5091.
(40) Urbas, A. M.; Sharp, R.; Fink, Y.; Thomas, E. L.; Xenidou, M.; Fetters, L. J. Tunable Block Copolymer/Homopolymer Photonic Crystals. *Adv. Mater.* **2000**, *12*, 812−814.
(41) Kang, Y.; Walish, J. J.; Gorishnyy, T.; Thomas, E. L. Broad-Wavelength-Range Chemically Tunable Block-Copolymer Photonic Gels. *Nat. Mater.* **2007**, *6*, 957−960.
(42) Kim, E.; Kang, C.; Baek, H.; Hwang, K.; Kwak, D.; Lee, E.; Kang, Y.; Thomas, E. L. Control of Optical Hysteresis in Block Copolymer Photonic Gels: A Step towards Wet Photonic Memory Films. *Adv. Funct. Mater.* **2010**, *20*, 1728−1732.
(43) Noro, A.; Tomita, Y.; Shinohara, Y.; Sageshima, Y.; Walish, J. J.; Matsushita, Y.; Thomas, E. L. Photonic Block Copolymer Films Swollen with An Ionic Liquid. *Macromolecules* **2014**, *47*, 4103−4109.
(44) Kang, C.; Kim, E.; Baek, H.; Hwang, K.; Kwak, D.; Kang, Y.; Thomas, E. L. Full Color Stop Bands in Hybrid Organic/Inorganic Block Copolymer Photonic Gels by Swelling−Freezing. *J. Am. Chem. Soc.* **2009**, *131*, 7538−7539.
(45) Runge, M. B.; Bowden, N. B. Synthesis of High Molecular Weight Comb Block Copolymers and Their Assembly into Ordered Morphologies in the Solid State. *J. Am. Chem. Soc.* **2007**, *129*, 10551−10560.
(46) Rzayev, J. Molecular Bottlebrushes: New Opportunities in Nanomaterials Fabrication. *ACS Macro Lett.* **2012**, *1*, 1146−1149.
(47) Rzayev, J. Synthesis of Polystyrene−Polylactide Bottlebrush Block Copolymers and Their Melt Self-Assembly into Large Domain Nanostructures. *Macromolecules* **2009**, *42*, 2135−2141.
(48) Xia, Y.; Olsen, B. D.; Kornfield, J. A.; Grubbs, R. H. Efficient Synthesis of Narrowly Dispersed Brush Copolymers and Study of Their Assemblies: The Importance of Side Chain Arrangement. *J. Am. Chem. Soc.* **2009**, *131*, 18525−18532.
(49) Sveinbjörnsson, B. R.; Weitekamp, R. A.; Miyake, G. M.; Xia, Y.; Atwater, H. A.; Grubbs, R. H. Rapid Self-Assembly of Brush Block Copolymers to Photonic Crystals. *Proc. Natl. Acad. Sci. U. S. A.* **2012**, *109*, 14332−14336.
(50) Miyake, G. M.; Piunova, V. A.; Weitekamp, R. A.; Grubbs, R. H. Precisely Tunable Photonic Crystals from Rapidly Self-Assembling Brush Block Copolymer Blends. *Angew. Chem., Int. Ed.* **2012**, *51*, 11246−11248.
(51) Piunova, V. A.; Miyake, G. M.; Daeffler, C. S.; Weitekamp, R. A.; Grubbs, R. H. Highly Ordered Dielectric Mirrors *via* the Self-Assembly of Dendronized Block Copolymers. *J. Am. Chem. Soc.* **2013**, *135*, 15609−15616.
(52) Macfarlane, R. J.; Kim, B.; Lee, B.; Weitekamp, R. A.; Bates, C. M.; Lee, S. F.; Chang, A. B.; Delaney, K. T.; Fredrickson, G. H.; Atwater, H. A.; Grubbs, R. H. Improving Brush Polymer Infrared One-Dimensional Photonic Crystals *via* Linear Polymer Additives. *J. Am. Chem. Soc.* **2014**, *136*, 17374−17377.
(53) Bockstaller, M. R.; Kolb, R.; Thomas, E. L. Metallodielectric Photonic Crystals Based on Diblock Copolymers. *Adv. Mater.* **2001**, *13*, 1783−1786.
(54) Bockstaller, M. R.; Thomas, E. L. Optical Properties of Polymer-Based Photonic Nanocomposite Materials. *J. Phys. Chem. B* **2003**, *107*, 10017−10024.
(55) Song, D.-P.; Li, C.; Colella, N. S.; Lu, X.; Lee, J.-H.; Watkins, J. J. Thermally Tunable Metallodielectric Photonic Crystals from the Self-Assembly of Brush Block Copolymers and Gold Nanoparticles. *Adv. Opt. Mater.* **2015**, *3*, 1169−1175.
(56) Beaulieu, M.; Hendricks, N.; Watkins, J. J. Large-Area Printing of Optical Gratings and 3D Photonic Crystals Using Solution-Processable Nanoparticle/Polymer Composites. *ACS Photonics* **2014**, *1*, 799−805.
(57) Howell, I. R.; Li, C.; Colella, N. S.; Ito, K.; Watkins, J. J. Strain-Tunable One Dimensional Photonic Crystals Based on Zirconium Dioxide/Slide-Ring Elastomer Nanocomposites for Mechanochromic Sensing. *ACS Appl. Mater. Interfaces* **2015**, *7*, 3641−3646.
(58) Song, D.-P.; Li, C.; Colella, N. S.; Xie, W.; Li, S.; Lu, X.; Gido, S.; Lee, J.-H.; Watkins, J. J. Large Volume Self-Organization of Polymer/Nanoparticle Hybrids with Millimeter Scale Grain Sizes Using Brush Block Copolymers. *J. Am. Chem. Soc.* **2015**, *137*, 12510−12513.
(59) Bolton, J.; Bailey, T. S.; Rzayev, J. Large Pore Size Nanoporous Materials from the Self-Assembly of Asymmetric Bottlebrush Block Copolymers. *Nano Lett.* **2011**, *11*, 998−1001.
(60) Buonsanti, R.; Pick, T. E.; Krins, N.; Richardson, T. J.; Helms, B. A.; Milliron, D. J. Assembly of Ligand-Stripped Nanocrystals into Precisely Controlled Mesoporous Architectures. *Nano Lett.* **2012**, *12*, 3872−3877.

DOI: 10.1021/acsnano.5b06525
ACS Nano 2016, 10, 1216−1223